JACOBS
UNIVERSITY

# Receiver Optimization of the L-Band Digital Aeronautical Communication System

by

**Ahmed Elshahed**

A thesis submitted in partial fulfillment

of the requirements for the degree of

**Master of Science**
**in Electrical Engineering**

Supervisor:

**Prof. Dr.-Ing. Werner Henkel**
Jacobs University Bremen

**Abstract**

In this thesis, we consider the interference cancellation problem for the broadband digital aeronautical communication system. We investigate the L-band digital aeronautical communication system (L-DACS) in the presence of distance measuring equipment (DME) interference. First, we describe the OFDM receiver of the LDACS1. In addition, we discuss the impacts of the DME spectrum on the subcarriers of the L-DACS1.

Then, we briefly point out the mitigation methods for canceling the effects of DME interference signals.

To model the impacts of DME interference at the L-DACS1 receiver, we adopt a Gaussian mixture (GM) model for impulse noise superimposed to additive white Gaussian noise (AWGN). Thus, we obtain the statistical parameters of the GM model in terms of the energy and duration of DME pulses.

Based on this modeling, we introduce a receiver optimization step of the L-DACS1 in the presence of DME interference. Herewith, we realize the optimum detector of OFDM systems in GM noise to cancel out the effect of DME interference.

# Acknowledgment

This work is the result of my research in the transmission system group at Jacobs University Bremen, Germany.

Foremost, I would like to express my deepest thanks to my supervisor Prof. Dr.-Ing. Werner Henkel. I am using this opportunity to express my gratitude to Dr K. A. Saaifan who supported me throughout my thesis, i am thankful for his aspiring guidance, invaluably constructive criticism and friendly advice during the thesis work. Last but not the least, I would like to thank my family for supporting me spiritually throughout my life and for their wise counsel and sympathetic ear. You are always there for me. Finally, there are my friends. We were not only able to support each other by deliberating over our problems and findings, but also happily by talking about things other than just our papers.

Thank you very much everyone.

# Statutory Declaration

(on Authorship of a Dissertation)

I, Ahmed Elshahed hereby declare that I have written this MSc thesis independently, unless where clearly stated otherwise. I have used only the sources, the data and the support that I have clearly mentioned. This MSc thesis has not been submitted for conferral of degree elsewhere.

I confirm that no rights of third parties will be infringed by the publication of this thesis.

Bremen,

Signature _____

# Dedication

*To my late father and my mother*

# Contents

# List of Figures

# Chapter 1

# Introduction

The L-DACS1 is a broadband candidate for the future L-Band digital aeronautical communication system (L-DACS). This system is proposed by the German Aerospace Center (DLR) to be replace the analog counterpart. The physical layer of the L-DACS1 system uses the orthogonal frequency-division multiplexing (OFDM) scheme to transmit digital data on multiple carrier frequencies. The frequency-division duplex (FDD) is also employed to separate a forward link (FL) and the reverse link (RL).
The aeronautical part of the L-band is mainly utilized by a distance measuring equipment (DME) and a tactical air navigation (TACAN) system. These systems are used to determine the slant range between an airborne and a ground station. For an efficient use of bandwidth in the L-band, the LDACS1 is developed as an inlay system between two adjacent channels used by DME ground stations. There are many challenges for the inlay approach: 1) The L-DACS1 signals must not disturb the existing L-band system. 2) The L-DACS1 received signals are subject to strong interference originating from the DME/TACAN systems. The out-of-band interference of the L-DACS1 signal towards the licensed DME/TACAN systems have been treated and studied in [1]. However, to guarantee reliable communications, the L-DACS1 receiver should possess an efficient cancellation scheme of DME/TACAN signals. Since the DME signals are characterized by random short pulses, the conventional pulse clipping and blanking techniques are applied to the l-DACS1 [2, 3]. Several methods including coding schemes and frequency domain pulse clipping are considered in [2, 4]. In this thesis, we model the DME interference to optimize the L-DACS1 receiver.

## 1.1 Outline of the Thesis

The rest of this thesis is organized as follow.

**Chapter 2**

We provide a brief introduction on the L-DACS1 system model. Thus, we present the OFDM receiver of the LDACS1 in the presence of DME interference. Additionally, we discuss the impacts of DME interference on the L-DACS1. Then, we briefly point the mitigation methods for canceling the effects of DME signals

In **Chapter 3**,

We investigate a Gaussian mixture (GM) model to model the impacts of DME interference at the L-DACS1. This model provides the probability density function (PDF) of the received interference plus background Gaussian noise.

**Chapter 4**

We consider the receiver optimization step of the L-DACS1 system in the presence of DME interference.

In 5, we conclude this thesis and provide future research directions.

# Chapter 2

# L-DACS1 System Model

In this chapter we provide a brief introduction on the L-DACS1 system model. Thus, we present the OFDM receiver of the LDACS1 in the presence of DME interference. Additionally, we discuss the impacts of DME interference on the L-DACS1. Then, we briefly point the mitigation methods for canceling the effects of DME signals.

## 2.1 L-DACS1 Physical Layer

The L-DACS1 physical layer is based on OFDM modulation, which was designed to operate in the aeronautical L-band ($960 - 1164$ MHz) as illustrated in Fig. 2.1. L-DACS1

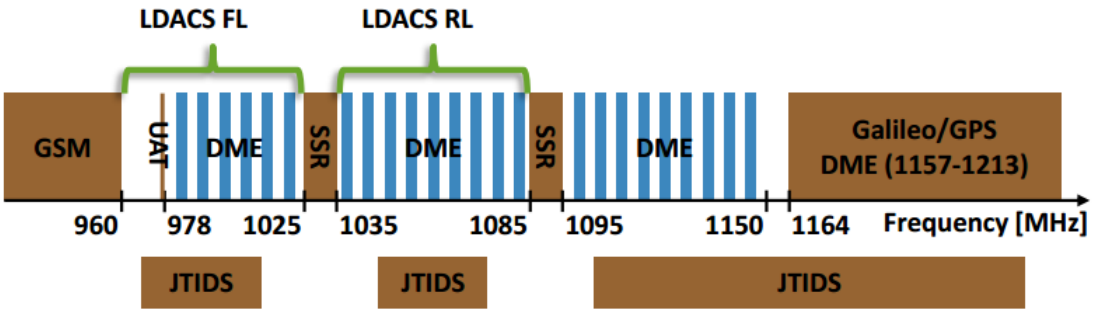


Figure 2.1: Current L-band usage

FL and RL are separated by a FDD scheme. In FL, the OFDM system is developed for packet switching networking users. The OFDM spectrum of L-DACS1 is constructed as an inlay system between two adjacent DME channels. A detailed physical layer description including all relevant OFDM parameters is given in Table 2.1.

Table 2.1: OFDM Parameters

| **Parameters** | **Values** |
|---|---|
| **Bandwidth** | 500 kHz (FL or RL) |
| **Sub-carrier spacing** | $\Delta f = 10.416$ kHz |
| **Used sub-carriers** | 48 |
| **FFT length** | $N = 64$ |
| **OFDM symbol duration** | 96 $\mu$s ($1/\Delta f$) |
| **Cyclic prefix** | 24 $\mu$s |
| **Total OFDM symbol duration** | $T_s = 120$ $\mu$s |
| **OFDM symbols per frame** | 54 |
| **Data OFDM symbols per frame** | 48 (FL) and 50 (RL) |
| **OFDM frame duration** | 6.48 ms |
| **Modulation** | QPSK |

According to these parameters, a bandwidth of 500 kHz is considered to be available for each L-DACS1 channel (FL or RL), with 48 sub-carriers used for data transmission. A fast Fourier transform (FFT) of length 64 is used with 8 guard sub-carriers on the left and the right side of the spectrum for filtering purposes. The guard interval (cyclic prefix) consumes 20% of the overall OFDM symbol duration. One half of the guard interval is used as conventional guard time to avoid inter-symbol interference between successive OFDM symbols. The other half is used for transmit-pulse shaping in order to decrease out-of-band radiation.

To relate the L-DACS1 parameters to the underlaying OFDM system, we consider an OFDM system with $N$ subcarriers and a symbol length of $T$ seconds. The $N$-subcarriers are given by

$$f_k(t) = \frac{1}{\sqrt{T}} e^{j2\pi k\Delta f t}, \quad 0 < t < T, \quad k = 0, 1, ...., N-1, \tag{2.1}$$

which represents a rectangular pulse modulated at the $k^{th}$ subcarrier, $k\Delta f$. Referring to Table 2.1, the subcarrier spacing is given as $\Delta f = \frac{500}{48} = 10.416$ kHz. Actually, the B-L-DACS1 system left 8 subcarriers at each side of the spectrum. Thus, the total number of subcarriers is $N = 64$. Therefore the bandwidth of OFDM signal is $W_S = N\Delta f = 666.624$ kHz. The OFDM symbol can be expressed in terms of $f_k(t)$, $k = 0, .., N-1$, as follows:

$$s(t) = \sqrt{\frac{E_b}{T}} \sum_{k=0}^{N-1} X_k e^{j2\pi k\Delta f t}, \quad 0 < t < T, \tag{2.2}$$

where $X_k$, $k = 0, 1, ...., N-1$, represent the transmit data symbols taken from a set of complex valued signal constellation points.

## 2.2 DME/TACAN System

The aeronautical part of the L-band, i.e. 960 - 1164 MHz, is reserved for the DME and the TACAN system. Both systems are being used for determining the slant range between an aircraft and a ground station as illustrated in Fig. 2.2. An aircraft interrogator sends

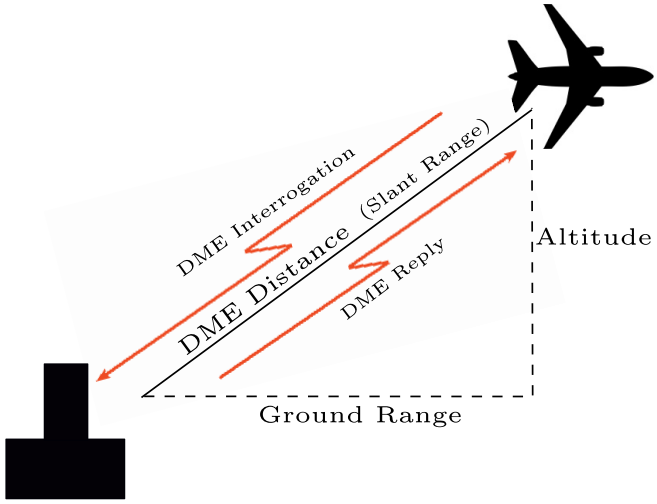


Figure 2.2: The DME system

a random sequence of pulse pairs (Gaussian) to a ground station that responds with the same sequence after a certain delay at a fixed frequency offset ±63 MHz. By measuring the elapsed time between the interrogation and the received reply from the ground station, the aircraft computes the distance to the ground station. To determine its exact position, the aircraft interrogates multiple ground stations and triangulates the measurement results. The DME signal consists of pairs of Gaussian-shaped pulses with spacing Δt. The baseband DME pulse pairs can be given by

$$d(t) = e^{-\varepsilon/2t^2} + e^{-\varepsilon/2(t-\Delta t)^2} \,. \tag{2.3}$$

The parameter $\varepsilon$=4.5.10$^{11}$ $1/s^2$ is set such that the time interval between the 50% amplitude point on leading and trailing edges of the pulse envelope is 3.5 $\mu$s. The spacing $\Delta t$ between the two pulses depends on the DME transmission mode, which varied from 12 $\mu$s to 36 $\mu$s. In our analysis, we consider the X mode with $\Delta t = 12\,\mu$s as illustrated in Fig. 2.4. The DME system operates in the aeronautical L-band from $960 - 1215$ MHz

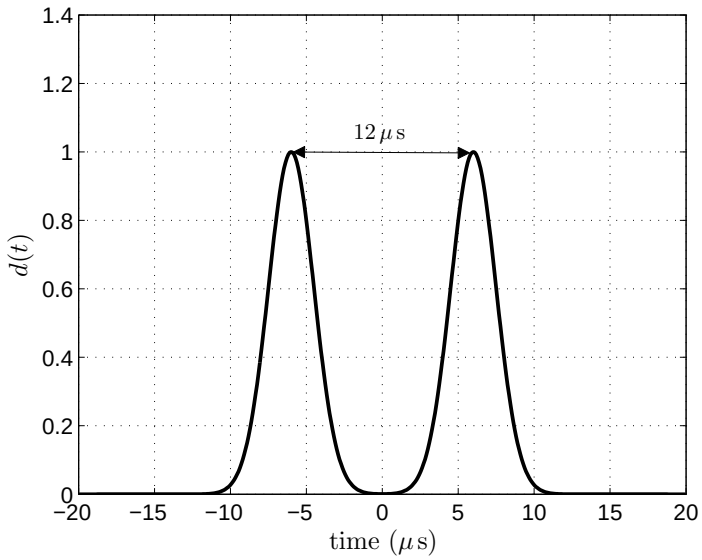


Figure 2.3: Guassian pulse pair of a DME signal

with a 1 MHz channel grid. The L-DACS1 utilizes the spaces of the 1 MHz grid of the DME channels in the L-band as illustrated in Fig. **??**. The center frequency of the OFDM

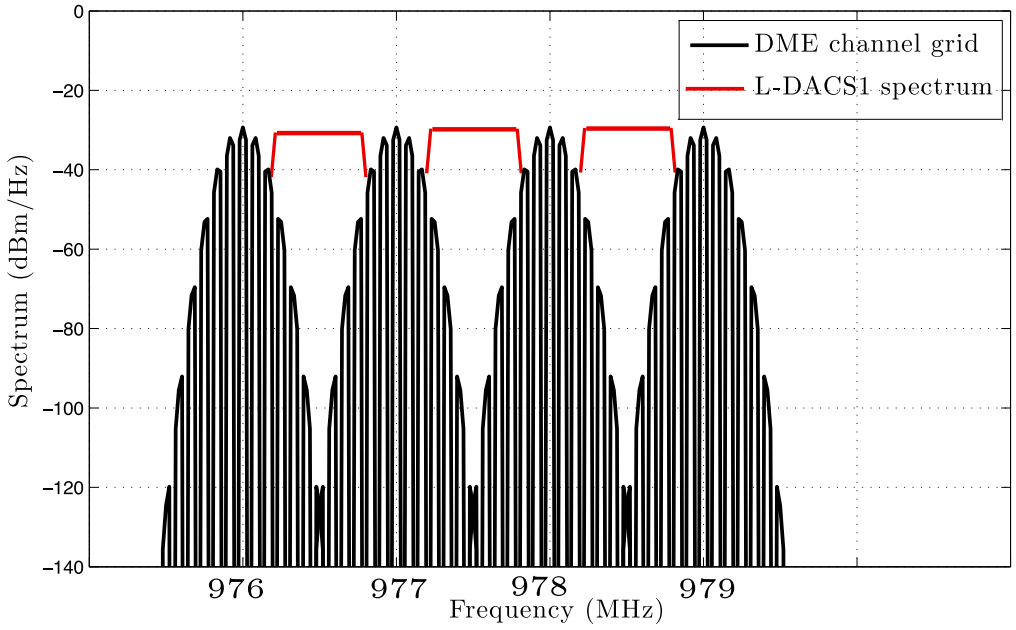


Figure 2.4: The 1 MHz grid of DME channels in the L-band

system of the L-DACS1 is located at the center between two consecutive DME channels. Thus, the DME signal is modulated at frequencies of the channels to the left and to the right of the OFDM system, i.e ±0.5 MHz, with the center frequency of the the OFDM system, at 0 Hz.

According to [4], the worst case scenario shows that the L-DACS1 is operating at 995.5 MHz and there is an interferer at −0.5 MHz offset to the L-DACS1 center frequency with interference power −67.9 dBm. In addition, there are two other interferers with peak powers −74 and −90.3 dBm are operating at +0.5 MHz offset to the L-DACS1 center frequency. Table 2.2 summarizes the characteristics of the received DME signal for the worst case scenario.

Table 2.2: Interference Scenario

| **Offset Frequency** | **Interference Power** | **Duty Cycle (ppps)** |
|---|---|---|
| −0.5 MHz | −67.9 dBm | 3600 |
| +0.5 MHz | −74 dBm | 3600 |
| +0.5 MHz | −90.3 dBm | 3600 |

## 2.3 The Impacts of the DME System on the L-DACS1

The impact of the DME system observed at the OFDM receiver is composed of contributions from $M$ DME stations operating in the same or different DME channels. The duty cycle of each DME station is considered by generating $L_m$, $m = 1, \cdots, M$, pulse pairs in the considered time interval for the $m^{\text{th}}$ DME station. The starting times $\tau_{m,l}$, $l = 1, \cdots, L_m$, of the pulse pairs for the $m^{\text{th}}$ DME station are modeled as a Poison process, which reflects the random behavior of the DME signal as interference. The phases $\varphi_{m,l}$ are equally distributed in the interval [0,2$\pi$]. The received interference power is taken into account by loading each pulse pair with peak power $P_m$, $m = 1, \cdots, M$. The resulting interference signal given by

$$i(t) = \sum_{m=1}^{M} \sum_{l=1}^{L_m} \sqrt{P_m} d(t - \tau_{m,l}) e^{j2\pi f_{c,m} t + j\varphi_{m,l}} , \tag{2.4}$$

where $f_{c,m}$ is the offset frequency of $m^{\text{th}}$ DME station from the center frequency of the the OFDM system.

To simulate the impact of DME interference on the L-DACS1, we adopt the DLR model as illustrated in Fig. 2.5. In this model, the arrival times of the DME/TACAN pulse pairs, $d(t)$, for each DME station can be modeled by a Poisson process with a rate $\lambda$ ppps. These pulse pairs are modulated to carrier frequencies corresponding to the center frequency of the channel where the regarded DME system is operated. For the considered OFDM parameters, the center frequency of the baseband L-DACS1 system is given by, $f_C = W_s/2 = 333.3$ kHz. According to the DLR recommendation, at the L-DACS1

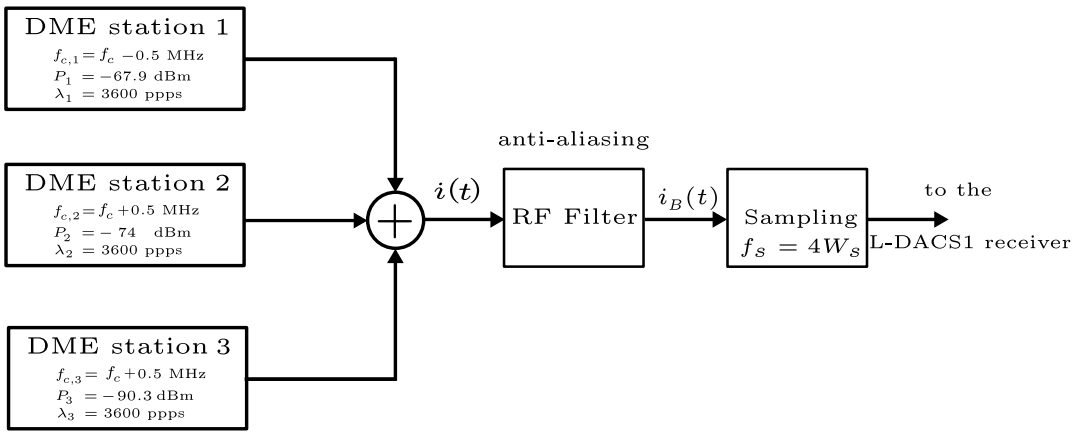


Figure 2.5: A block diagram of interference simulator

receiver, the desired signal and the interference are passed through a received RF filter [3]. Then, the received signal is sampled and processed to the OFDM receiver of the L-DACS1 system. The continues-time received signal can be expressed as

$$y(t) = s(t) + w(t) + i_B(t)\,, \quad 0 \le t \le T\,, \tag{2.5}$$

where $s(t)$ is the desired OFDM symbol. $w(t)$ is a baseband additive white Gaussian noise (AWGN) signal with zero mean and variance $\sigma^2 = N_0 W_s$. $i_B(t)$ represents the impacts of DME interference at the L-DACS1 receiver. In order to avoid the aliasing effects of interference, the received signal is sampled at a sampling rate, $f_s = 4 \times W_s$. As in [2, 5], we apply a receive windowing, which reduces the additional effects of DME pulses that do not coincide completely within the duration of one OFDM symbol. Due to the design of the windowing, only the interference part of the received signal is affected, whereas the data part of the received signal is not changed at all. After sampling, i.e., $t = n/f_s$, the received samples after CP removal are given as

$$y[n] = s[n] + w[n] + i_B[n]\,, \quad n = 0, \cdots, 4N-1\,, \tag{2.6}$$

where

$$s[n] = \sqrt{\frac{E_b}{T}} \sum_{k=0}^{4N-1} x_k e^{j2\pi kn/4N}\,, \quad n = 0, \cdots, 4N-1\,, \tag{2.7}$$

denotes the 4-times oversampled OFDM symbol. The block diagram of the OFDM signal processing is depicted in Fig. 2.6. Similar to the conventional OFDM system, the sampled signal is transformed to the frequency domain by means of a $4N$-point FFT. The larger FFT length is required because of 4-times oversampling. Thus, the received subcarriers

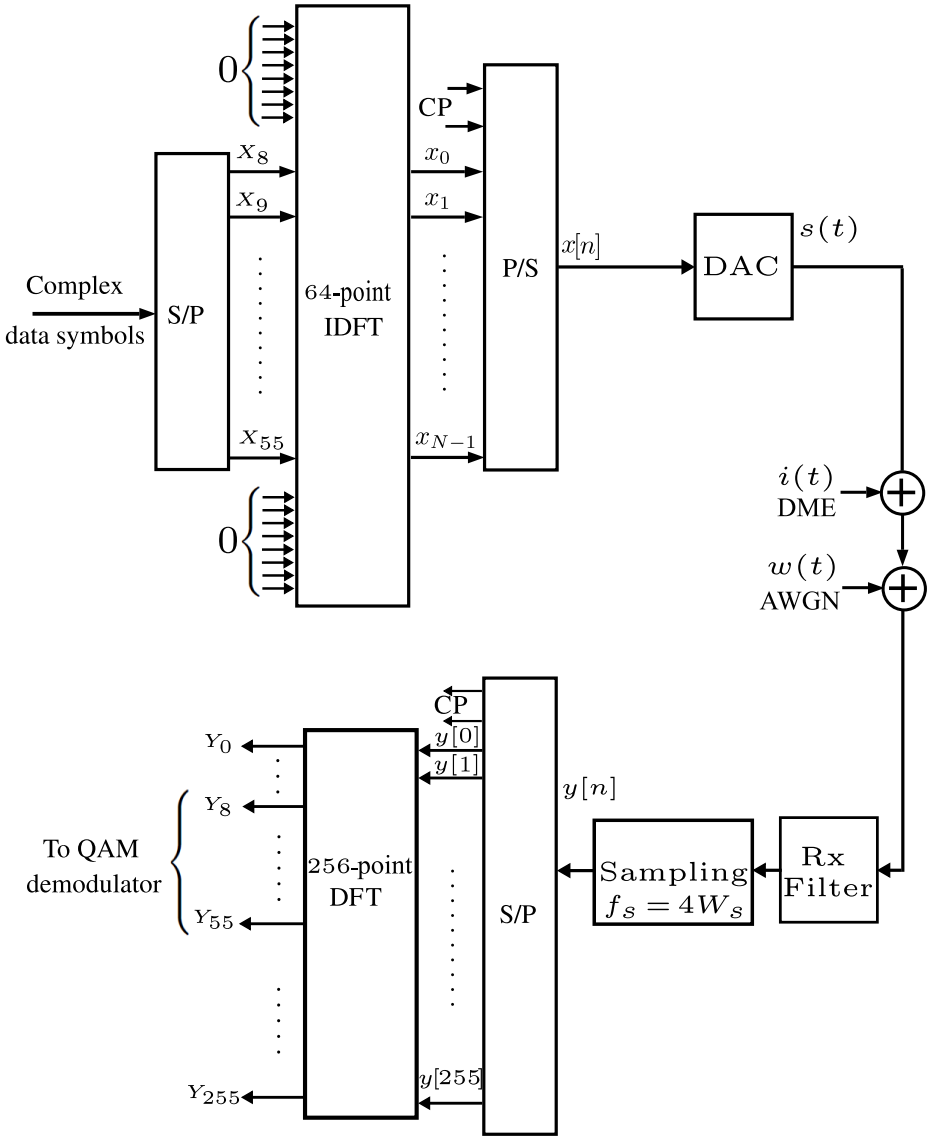


Figure 2.6: The L-DACS1 OFDM system

can be expressed as

$$Y_k = \frac{1}{\sqrt{T}} \sum_{k=0}^{4N-1} y[n] e^{-j2\pi \frac{kn}{4N}} , \tag{2.8}$$

$$= \sqrt{E_b} X_k + W_k + I_{b,k} , \quad k = 0, \cdots , 4N-1 , \tag{2.9}$$

where $W_k$ is the AWGN sample of the $k^{\text{th}}$ subcarrier. Since the FFT is unitary, $W_k$ is Gaussian with zero mean and variance $N_0$. The sample $I_{b,k}$ represents the impacts (spectrum) of the DME signal on the $k^{\text{th}}$ subcarrier. The part relevant for the L-DACS1 receiver is extracted at the subcarriers index, $k = 8, \cdots , 55$. Hence, the contribution of the interference to each OFDM subcarrier is obtained.

To illustrate the impact of a DME interference on an L-DACS1 receiver, we considered a severe interference scenario described in Table 2.2. The pulse rates of the interferers superimpose such that almost every OFDM symbol is affected by at least one pulse pair. Figure 2.7 depicts the power spectrum density of the received interference (DME signal and AWGN). The interfering signals are randomly generated for 1500 OFDM frames

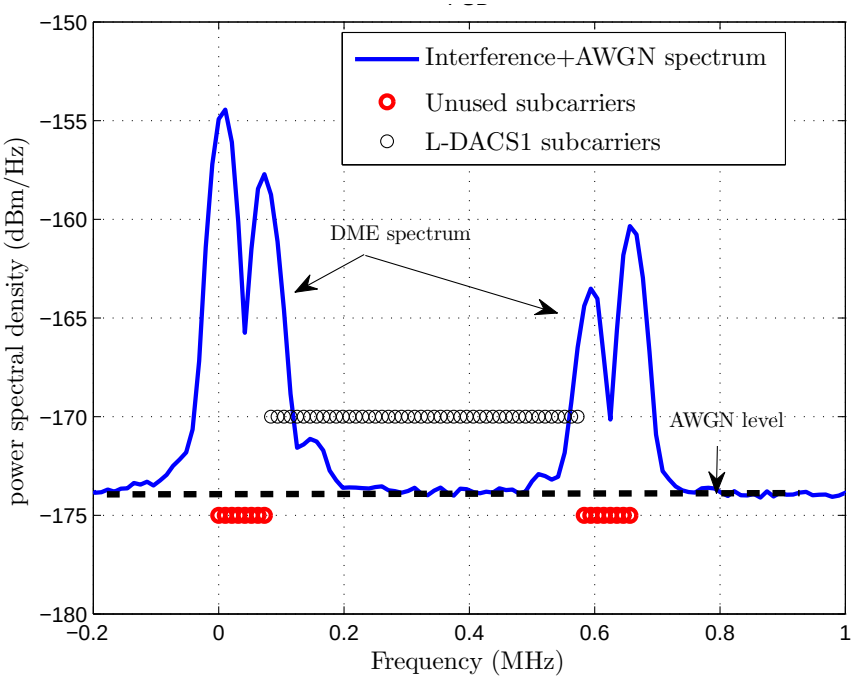


Figure 2.7: The impacts of DME interference and AWGN on the L-DACS1

and the resulting power spectral are averaged over all trials. We can see that the outer subcarriers of the L-DACS1 system are subject to a strong interference effect, which limits performance of the L-DACS1 system.

Mainly, two approaches are developed to reduce the effects of DME interference on the L-DACS1 system [3]. Figure 2.8 illustrates a time-domain approach and a frequency-domain

approach in the presence of DME interference. The time-domain approach reduces the

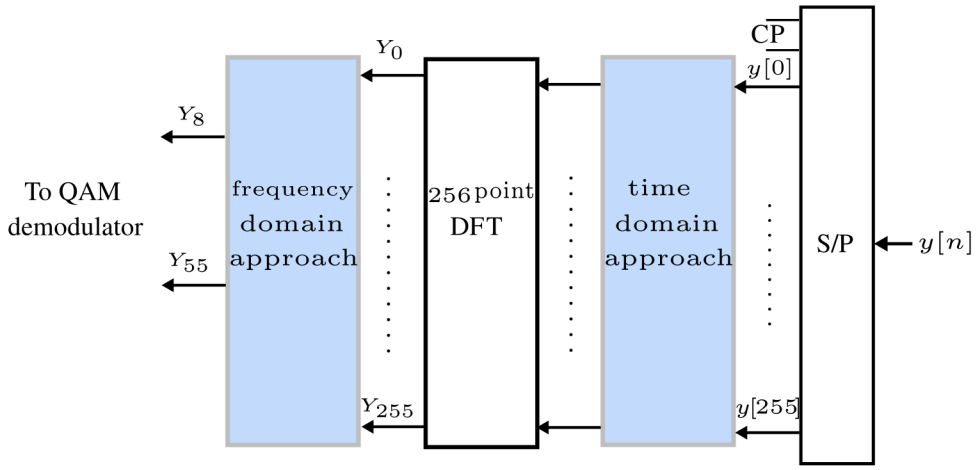


Figure 2.8: DME mitigation schemes for the L-DACS1

effect of a DME signal before the FFT operation (time direction) such as a pulse clipper or pulse blanker [6]. These schemes suffer from a drawback that the desired signal is either clipped or blanked. Furthermore, the pulse blanking method inserts intercarrier interference in an OFDM system [6]. The frequency-domain approach reduces the DME spectrum impacts on the victim subcarriers. Since the DME spectrum hits the outer subcarriers of the L-DACS1 system, this approach applies many schemes to correct the unreliable information of the impaired subcarriers.

# Chapter 3

# Statistical Modeling of DME Interference

Although the DME signal is deterministic, the DME interference has impulse appearances at the L-DACS1 system. One of the essential steps in receiver optimization in impulse noise is the statistical modeling of received interference. In this chapter, we investigate a Gaussian mixture (GM) model to model the impacts of DME interference at the L-DACS1. This model provides the probability density function (PDF) of the received interference plus background Gaussian noise.

## 3.1 The GM Model for Impulse Noise

The GM model is proved to model impulse noise measured at a 2.4 GHz wireless band [6]. This model assumes that the received interference, $z(t) = w_G(t) + w_I(t)$, consists of two components: a Gaussian component $w_G(t)$ and an impulsive component $w_I(t)$. The Gaussian component represents AWGN, which has a flat power spectral density $N_0$ Watt/Hz. However, the impulsive component models the presence of impulsive noise, which can be characterized by Gaussian samples during an active pulse interval $T_I$. Figure 3.1 depicts a pictorial picture of impulse noise modeled by the GMM. We observe that the appearance of impulse noise is similar to a rectangular pulse signal with duty cycle $A = \frac{T_I}{T}$, where $1/T$ gives the rate of impulse noise. The impulsive samples during the impulse active time, $T_I$, have a flat energy spectral density $I_p$ W/Hz. In Fig. 3.2 we depict the power spectral density of the baseband received interference as seen by the receiver. The GMM uses two scaled joint Gaussian densities to model the quadrature

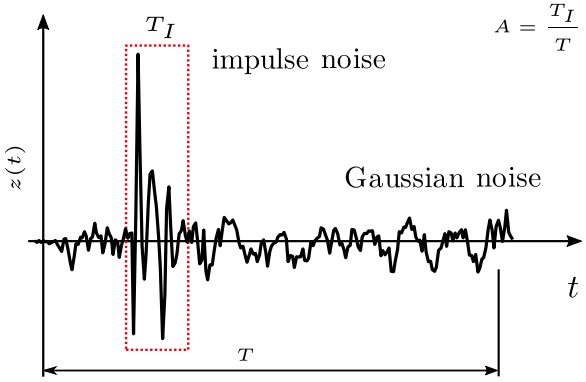


Figure 3.1: A pictorial view of impulse noise

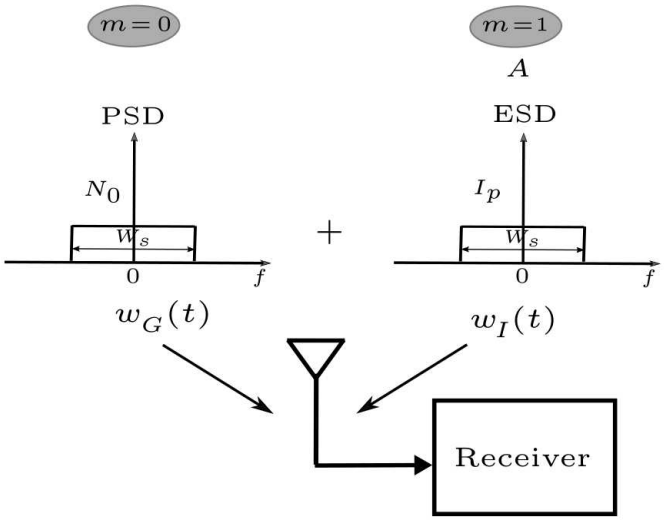


Figure 3.2: The GMM for impulse interference as seen by the receiver

components of the received interference, $z(t)$. Since $z(t) = \mathrm{Re}\{z(t)\} + j\mathrm{Im}\{z(t)\}$. The GMM distribution is given as

$$p_z(z) = \frac{1-A}{\pi\sigma_0^2}\mathrm{e}^{-|z|^2/\sigma_0^2} + \frac{A}{\pi\sigma_1^2}\mathrm{e}^{-|z|^2/\sigma_1^2}\,, \tag{3.1}$$

where $\sigma_0^2 = \mathrm{E}[|w_G(t)|^2] = N_0 W_s$ is the variance of the background component. However, the second component models the presence of impulse noise. Thus, the variance $\sigma_1^2 = N_0 W_s + I_p W_s$ represents the sum of variances of the Gaussian noise and impulsive noise.

## 3.2 DME Pulse Analysis

In this analysis, we consider a single DME station operating with an offset frequency $f_{c,m}$, a peak power $P_m$, and a pulse rate $\lambda_m$. In Figure (3.3), we depict the baseband model of the DME interference at the L-DACS1 receiver. For simplicity, we consider a single DME pulse pairs which can be given by

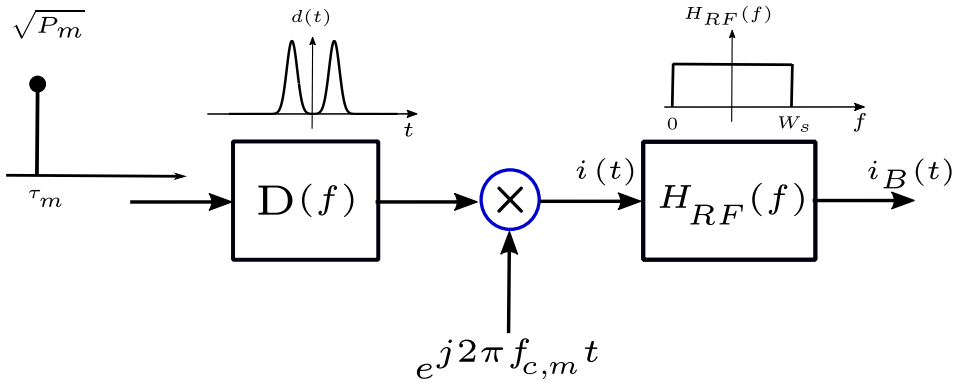


Figure 3.3: The baseband model for DME interference at the L-DACS1 system

$$i(t) = \sqrt{P_m}d(t-\tau_m)e^{j2\pi f_{c,m}t}\,, \tag{3.2}$$

where $\tau_m$ is the random delay the DME pulse pairs, $d(t)$. The Fourier transform of $i(t)$ can be give as follows:

$$I(f) = \sqrt{P_m}D(f-f_{c,m})e^{-j2\pi f\tau_m}\,, \tag{3.3}$$

where $D(f)$ is the Fourier transform of $d(t)$, which can be given as

$$D(f) = 2\sqrt{\frac{2\pi}{\alpha}}e^{-\frac{2\pi^2}{\alpha}f^2}\cos(\pi f\Delta t)e^{-j\pi f\Delta t}\,, \tag{3.4}$$

where $\Delta t = 12\,\mu$s for the X mode operation of the DME station. The energy of a single Gaussian pairs is given as

$$E_{gpp} = P_m \int_{-\infty}^{+\infty} |d(t)|^2 dt = P_m \int_{-\infty}^{+\infty} |D(f)|^2 df\,,$$
$$= 2\sqrt{\frac{\pi}{\alpha}} P_m\,. \tag{3.5}$$

Thus, the average power of the DME interference, $i(t)$, operates with pulse rate $\lambda_m$ can be given as

$$P_{av,m} = 2\sqrt{\frac{\pi}{\alpha}} P_m \lambda_m\,. \tag{3.6}$$

The impacts of the DME interference is given by passing $i(t)$ through a received filter, $H_{RF}(t)$. Figure 3.4 illustrates the transfer function of the received filter obtained from the DLR specifications [7]. The spectrum of the filtered DME interference, $i_B(t)$, can be

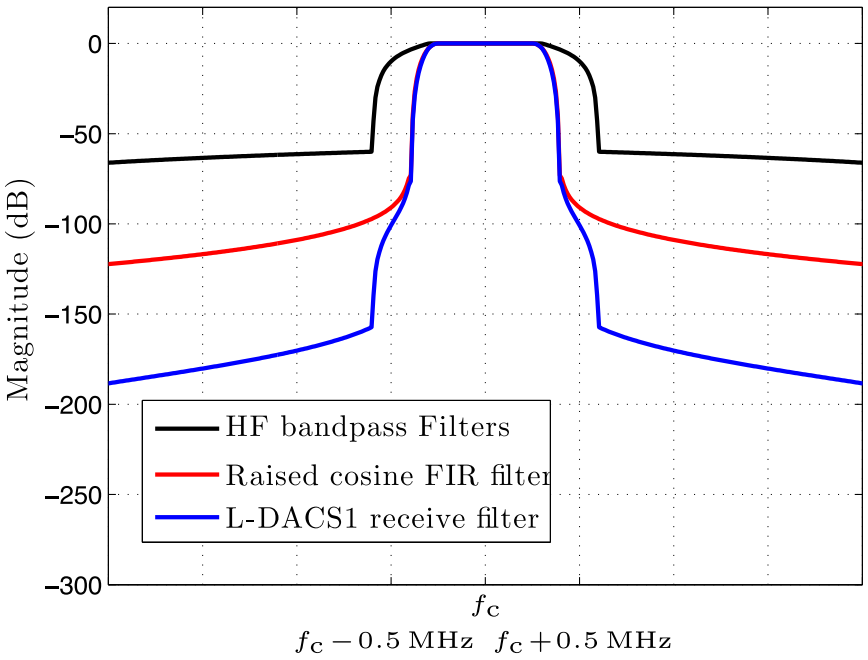


Figure 3.4: The L-DACS1 receive filter

expressed as

$$I_B(f) = \sqrt{P_m} D(f - f_{c,m}) H_{RF}(f) e^{-j2\pi f \tau_m} \tag{3.7}$$

Ideally, the received filter, $H_{RF}(f)$, should pass the baseband spectrum of the L-DACS1 system centered at $f_c = 333.3$ kHz. Since $f_{c,m}$ is the offset frequency of DME interference

from $f_c$, the energy of the filtered Gaussian pulse pairs can be evaluated as

$$E_B = P_m \int_0^{W_s} |D(f - f_{c,m})|^2 df = P_m I_{gpp}\,, \tag{3.8}$$

For $f_{c,m} = f_c \pm 0.5\,\text{MHz}$, the term $I_{gpp}$ can be evaluated as $\int_0^{W_s} |D(f - f_{c,m})|^2 df = 3.5 \times 10^{-8}$. Figure illustrates the energy spectral density of the impacts of DME interference operates at +0.5 MHz offset to the center frequency of the L-DACS1 receiver. This shows how the upper subcarriers of the L-DACS1 system are affected by strong impacts of a DME spectrum. To investigate these impacts on a received OFDM symbol, we look at

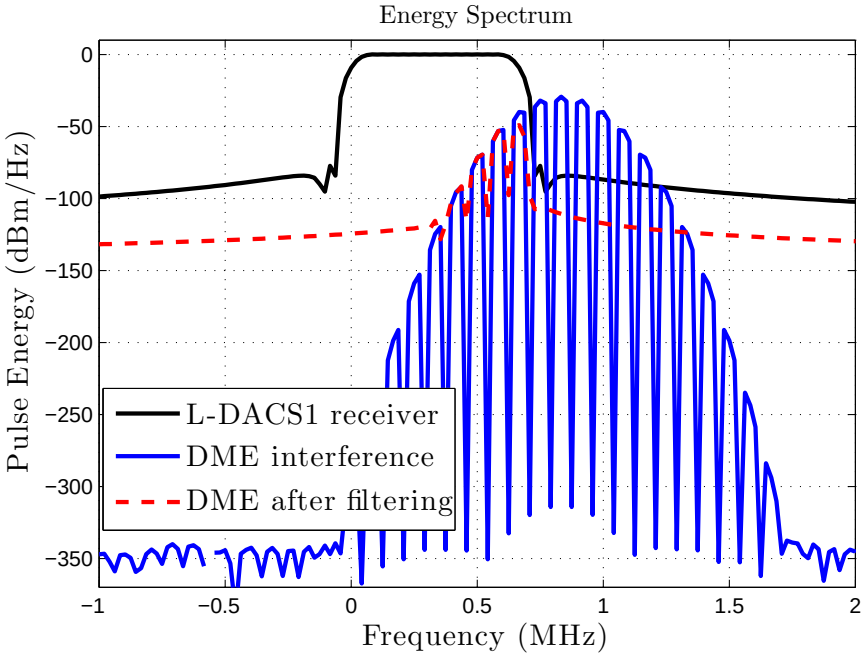


Figure 3.5: The L-DACS1 receive filter

the DME impacts on the time domain as illustrated in Fig. 3.6. Since $i_B(t)$ comprises of filtered quadrature components of $i(t)$, the figure shows the envelop $|i_B(t)|$ compared with the received OFDM symbol duration. We observe that the DME interference corrupt more than 25% of the received OFDM symbol.

## 3.3 The GMM for DME Interference

This section introduces the GMM as a statistical model for AWGN and the impacts of DME interference at the L-DACS1 receiver. First, we provide the modeling steps for a single DME interfering station. Then, we verify the GMM for the worst case scenario of

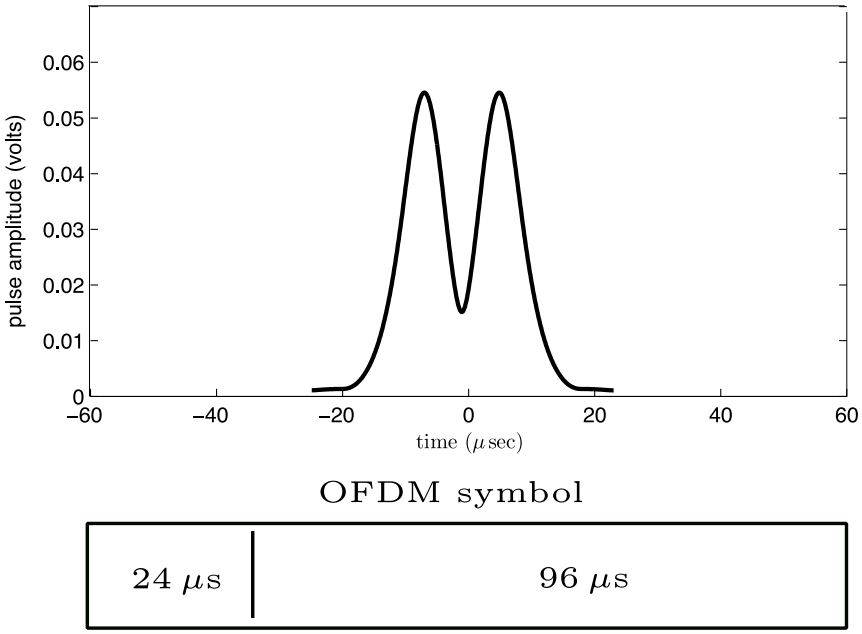


Figure 3.6: The impacts of DME interference on the OFDM symbol

the DME interference.

We consider a single DME station operating at an offset frequency $f_{c,1} = f_c + 0.5$ MHz and pulse rate $\lambda_1 = 10800$ ppps. The peak power of the DME signal is $P_1 = -70$ dBm. In Fig. 3.6, we observed that the appearance of DME interference is similar to impulse noise with active pulse time $T_I = 30\,\mu$s. Therefore, we use the GMM to model the received DME signal $i_B(t)$ plus the AWGN component $w_g(t)$. Since the baseband received interference $z(t) = w_g(t) + i_B(t)$ is given in a complex form, we use the baseband GMM as follows:

$$p_z(z) = \frac{1-A}{\pi\sigma_0^2}\mathrm{e}^{-|z|^2/\sigma_0^2} + \frac{A}{\pi\sigma_1^2}\mathrm{e}^{-|z|^2/\sigma_1^2}\ , \tag{3.9}$$

where the first component models $z(t)$ in the absence of DME interference. Then, the variance $\sigma_0^2 = N_0 W_s$ denotes the variance of the complex-valued AWGN, $w_g(t)$. However, the second component models the interference $z(t)$ in the presence of DME interference. Thus, the variance $\sigma_1^2 = N_0 W_s + P_I$ denotes the sum of the AWGN variance and DME interference power as seen by the L-DACS1 receiver. $A = \lambda_1 \times T_I$ represents the duty cycle of DME pulsed interference. The power of DME interference as seen by the L-DACS1 receiver can be related to the energy of the filtered DME pulse pair (given in (3.8)) as follows:

$$P_I = P_1 \times I_{gpp}/T_I\ , \tag{3.10}$$

where $I_{gpp} = 3.5 \times 10^{-8}$ is the energy of a filtered DME Gaussian pulse pairs and $A = \lambda_1 \times T_I$. Since the received interference $z(t)$ is a complex-valued baseband process, we

investigate the voltage histograms of in-phase and quadrature components of $z(t)$. In Fig. 3.7, we depicts the voltage histograms of the received interference (DME+AWGN) for a single DME station with an offset frequency $f_{c,1} = f_c + 0.5$ MHz, pulse rate $\lambda_1 = 10800$ ppps and peak power of the DME signal is $P_1 = -70$ dBm.

It is clear that the GM model provides a very good approximation for the PDF of the quadrature components of the received noise.

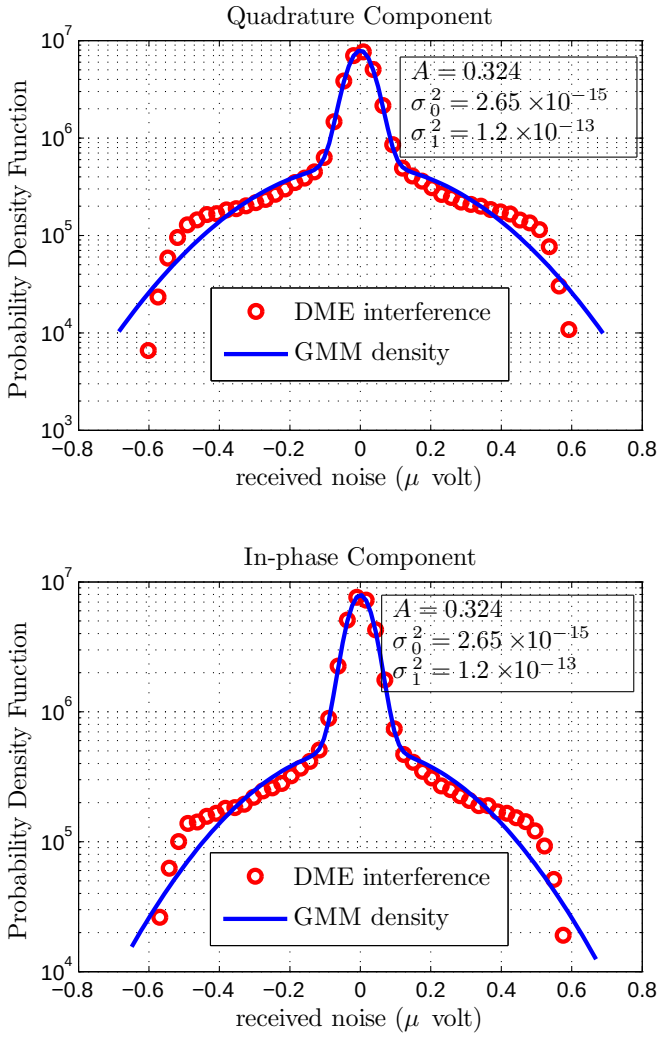


Figure 3.7: The GMM for the impacts of DME interference and AWGN for a single DME station

In general, the victim receiver is subject to several DME stations of different received

power $P_m$ and pulse rate $\lambda_m$. Herewith, we investigate the GM model with

$$A = \sum_{m=1}^{M} \lambda_m \times T_I \ , \tag{3.11}$$

and

$$P_I = 1/M \sum_{m=1}^{M} P_m \times I_{gpp}/T_I \ , \tag{3.12}$$

to model the impacts of the worst case scenario. As mention before, the parameters of the worst case scenario are listed in table 2.2. Figure 3.8 depicts the voltage histogram of the received interference and those for the GM model.

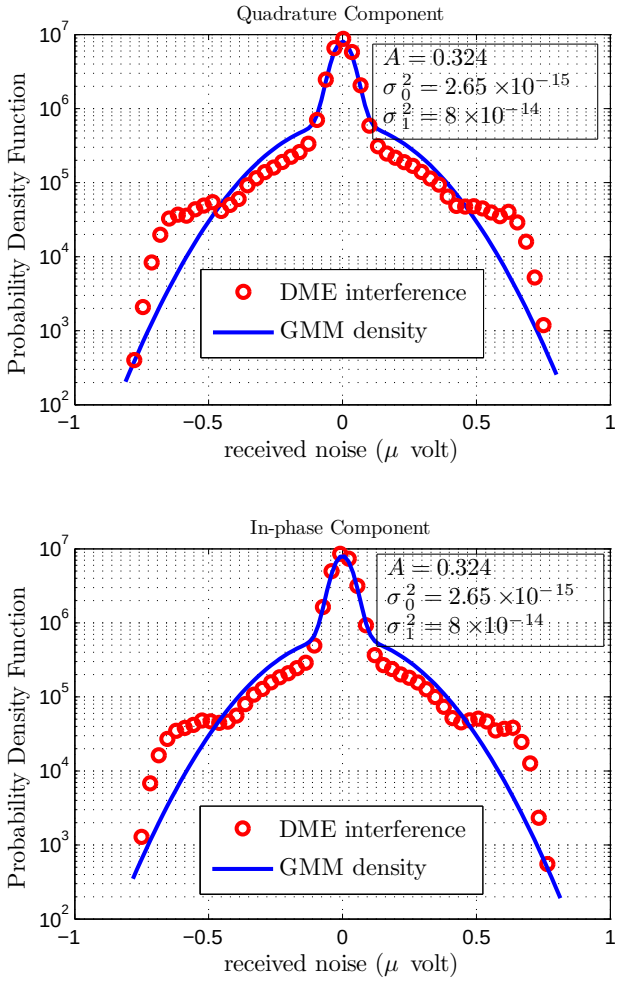


Figure 3.8: The GMM for the impacts of DME interference and AWGN for the worst case scenario

# Chapter 4

# Optimum Receiver Design for the L-DACS1 System

In this Chapter, we consider the receiver optimization step of the L-DACS1 system in the presence of DME interference.

## 4.1 Receiver Optimization

In the previous Chapter, we showed that the impacts of received DME interference and background Gaussian noise can be modeled by a GM model. Hence, one can see the L-DACS1 system as a multicarrier system with $N = 64$ subcarriers operate in GM interference. The received OFDM symbol after the CP removal can be represented by

$$\mathbf{y} = \sqrt{\frac{E_b}{T_s}}\mathbf{x} + \mathbf{z} \,, \tag{4.1}$$

where $E_b$ is the signal energy per bit and according to L-DACS1 parameters $T_s$ is the sampling interval, which can be given as $T_s = 1/W_s$. This means, we do not use an oversampling by factor 4 since we optimize the receiver in time domain. $\mathbf{x} = \mathbf{W}_N^H \mathbf{X}$ denotes an $N \times 1$ transmit OFDM symbol, where $\mathbf{W}_N^H$ is the IDFT matrix and where $\mathbf{X} \in \mathbb{C}^{N\times 1}$ represents the complex-valued data vector. $\mathbf{z} = \mathbf{w}_g + \mathbf{i}_B \in \mathbb{C}^{N\times 1}$ consists of the impacts of AWGN and DME interference at the L-DACS1 receiver. The elements of $\mathbf{z}$ are the samples of $z(t) = w_g(t) + i_B(t)$ sampled with $T_s$. Hence, we invoke the GM

model to approximate the PDF of the elements of $\mathbf{z}$ as

$$p(z_n) = \frac{1-A}{\pi\sigma_0^2} e^{-\frac{|z_n|^2}{\sigma_0^2}} + \frac{A}{\pi\sigma_1^2} e^{-\frac{|z_n|^2}{\sigma_1^2}} , \tag{4.2}$$

where $\sigma_0^2 = N_0 W_s$ and $\sigma_1^2 = N_0 W_s + \frac{1}{M}\sum_{m=1}^{M} P_m \cdot \frac{I_{gpp}}{T_I}$. So, we can see receiver optimization of the L-DACS1 as a detection problem of OFDM signals in GM interference. In the following sections, we introduce the optimum receiver design for the L-DACS1 system in DME interference.

## 4.2 The Optimum Receiver

The GM model describes only the amplitude distributions with almost no correlation properties in time direction. Since the DME pulse pairs are active for $T_I = 30\,\mu$s, $N_I = T_I/T_s = 20$ samples of the received OFDM signal are affected by DME interference. Thus, when DME interference is occurred, the samples of $\mathbf{z}$ possess $N_I$ jointly dependent observations. To simplify the analysis, we assume that the receiver knows the location of DME pulse pairs in time domain. To realize this assumption, one can utilizes time/frequency properties of DME signals to estimated the affected samples by impulsive interference [**?**, 6]. Thus, under this knowledge, the GM model reduces to a conditional Gaussian density as

$$p(z_n|l_n) = \frac{1}{\pi\sigma_{l_n}^2} e^{-\frac{|z_n|^2}{\sigma_{l_n}^2}} , \tag{4.3}$$

where $l_n = 0, 1$ are the Gaussian and impulsive states of a GM model. For a given noise state vector $\mathbf{l} = [l_0\, l_1 \cdots \overbrace{l_K \cdots l_{K+N_I-1}}^{\text{DME impulse}} \cdots l_{N-1}]$, the joint distribution of a noise vector $\mathbf{z} = [z_0\ z_1\ \cdots\ z_{N-1}]^T$ can be given as

$$p(\mathbf{z}|\mathbf{\Sigma}_z) = \frac{1}{\pi^N |\mathbf{\Sigma}_z|} e^{-\mathbf{z}^H \mathbf{\Sigma}_z^{-1} \mathbf{z}} . \tag{4.4}$$

The covariance matrix of the noise vector $\mathbf{z}$ is given by

$$\mathbf{\Sigma}_z = \mathrm{E}\left[\mathbf{z}\mathbf{z}^H\right] = \begin{pmatrix} \sigma_0^2 \mathbf{I}_{K\times K} & \mathbf{0}_{K\times N_I} & \mathbf{0}_{K\times N-K-N_I} \\ \mathbf{0}_{N_I\times K} & \mathbf{\Sigma}_I & \mathbf{0}_{N_I\times N-K-N_I} \\ \mathbf{0}_{N-K-N_I\times K} & \mathbf{0}_{N-K-N_I\times N_I} & \sigma_0^2 \mathbf{I}_{N-K-N_I\times N-K-N_I} \end{pmatrix} , \tag{4.5}$$

where $\mathbf{\Sigma}_I$ is an $N_I \times N_I$ covariance matrix of the $N_I$ consecutive noise samples impaired by DME interference. Therefore, the joint PDF of the received signal vector, $\mathbf{y}$, conditioned

on the transmitted information symbol, $\mathbf{X}$, is given by

$$p(\mathbf{y}|\mathbf{X}) = \frac{1}{\pi^N |\mathbf{\Sigma}_z|} e^{-\left(\mathbf{y}-\sqrt{\frac{E_b}{T_s}}\mathbf{W}_N^H\mathbf{X}\right)^H \mathbf{\Sigma}_z^{-1}\left(\mathbf{y}-\sqrt{\frac{E_b}{T_s}}\mathbf{W}_N^H\mathbf{X}\right)} , \tag{4.6}$$

The optimum detector selects the sequence that maximizes this quantity as follows

$$\hat{\mathbf{X}}_{\mathrm{ML}} = \underset{\mathbf{X}\in\mathbb{C}^{N\times 1}}{\arg\max}\, p(\mathbf{y}|\mathbf{X}) . \tag{4.7}$$

For antipodal information sequences, the optimum detector should search over $2^N$ possible choices of the bits in the transmitted signal vector $\mathbf{X}$. Since $\mathbf{\Sigma}_\mathbf{z}^{-1} = \mathbf{L}\mathbf{L}^H$, the ML estimate of the transmitted information symbol leads to

$$\hat{\mathbf{X}}_{\mathrm{ML}} = \arg\min_{\mathbf{X}} \left|\mathbf{L}^H\mathbf{y} - \sqrt{\tfrac{E_b}{T_s}}\mathbf{L}^H\mathbf{W}_N^H\mathbf{X}\right|^2 , \tag{4.8}$$

which searches over all possible information symbols to select a closest signal vector to the received vector $\mathbf{L}^H\mathbf{y}$. Additionally, the optimum detector requires perfect knowledge of DME pulse locations and the covariance matrix $\mathbf{\Sigma}_I$. For simplicity, we design the OFDM receiver for $\mathbf{\Sigma}_I = \sigma_1^2\mathbf{I}_{N_I\times N_I}$, which leads to an upper performance bound of the optimum receiver.

The optimum decision rule is equivalent to finding the closest lattice point to a received point $\mathbf{L}^H\mathbf{y}$. Thus, we use the lattice decoder to realize the optimum OFDM detector under perfect knowledge of DME pulse locations.The lattice decoder searches over all possible lattice points that lie within a sphere of radius $\beta_0$ around the received point $\mathbf{L}^H\mathbf{y}$. The sphere equation of the optimum detector can be expressed as

$$\left|\mathbf{L}^H\mathbf{y} - \mathbf{G}\mathbf{X}\right|^2 \leq \beta_0 , \tag{4.9}$$

where $\mathbf{G} = \sqrt{\frac{E_b}{T_s}}\mathbf{L}^H\mathbf{W}_N^H$. The sphere equation in (4.9) requires perfect knowledge of the noise states $l_n$, $n = 0, \cdots, N-1$, to compute $\mathbf{\Sigma}_\mathbf{z}^{-1} = \mathbf{L}\mathbf{L}^H$. Using a QR decomposition, the matrix $\mathbf{G}$ can be factorized into a product of a unitary matrix $\mathbf{Q}$ and an upper triangular matrix $\mathbf{R}$.Thus, (4.9) can be reduced as

$$\begin{aligned} \left|\mathbf{L}^H\mathbf{y} - \mathbf{Q}\mathbf{R}\mathbf{X}\right|^2 &\leq \beta_0 , \\ \left|\mathbf{Q}^H\mathbf{L}^H\mathbf{y} - \mathbf{Q}^H\mathbf{Q}\mathbf{R}\mathbf{X}\right|^2 &\leq \beta_0 , \\ \left|\mathbf{y}' - \mathbf{R}\mathbf{X}\right|^2 &\leq \beta_0 , \end{aligned} \tag{4.10}$$

which is identical to solving the following linear least squares problem

$$\sum_{j=n}^{N-1} \left| y_j' - \sum_{i=j}^{N-1} R_{j,i} X_i \right|^2 \leq \beta_0 \, , n = 0, \cdots, N-1 \, , \tag{4.11}$$

which denotes the problem of the lattice (sphere) decoder to finding the closest signal vector that satisfies the above set of conditions in the order from $n = N-1$ to $n = 0$. In the simulation results, we implement the K-best algorithm [8, 9] of lattice decoding for multicarrier systems in DME interference.

## 4.3 Simulation Results

To confirm the sphere decoder in treating the effects of DME interference for L-DACS1 system, we provide simulation results for two different interference scenarios. For the sake of comparisons, we additionally implement a clipping detector to cancel the impacts of DME pulses. Simply, the clipping detector limits the received amplitude to a certain threshold when the received signal exceeds this threshold. In [6], the clipping detector of the OFDM system in GM noise is given by

$$\hat{y}_n = \begin{cases} \frac{\sigma_s^2}{\sigma_s^2 + \sigma_0^2} y_n & \text{if } l_n = 0 \, , \\ \frac{\sigma_s^2}{\sigma_s^2 + \sigma_1^2} y_n & \text{if } l_n = 1 \, . \end{cases} \tag{4.12}$$

where $\sigma_s^2 = \mathrm{E}\{|s[n]|^2\} = \frac{E_b}{T_s}$. In the simulation results, we simulated the bit-error-ratio (BER) of the L-DACS1 system using binary phase shift-keying (BPSK) for OFDM systems in the presence of DME interference. In Fig. 4.1, we depict the BER performance of the sphere decoder for a single DME station with received peak power of 75 dBm and rate 10800 ppps. In addition, we show the BER of the conventional OFDM receiver and a clipping detector for L-DACS1 system in DME interference. We can see that the sphere decoder provides a close performance to the free interference case (a gap of 2 dB only), which realizes the sphere decoder for treating the effects of impulse noise [6, 7].

In Fig. 4.2, we depict the BER performance of the sphere decoder for the worst case scenario of DME interference, which is given in Table 2.2. From this figure, one can recognize that the gap in performance between the free interference limit (AWGN only) and the sphere decoder is almost 2 dB. This confirms the advantages of the sphere decoder to cancel the impacts of DME interference

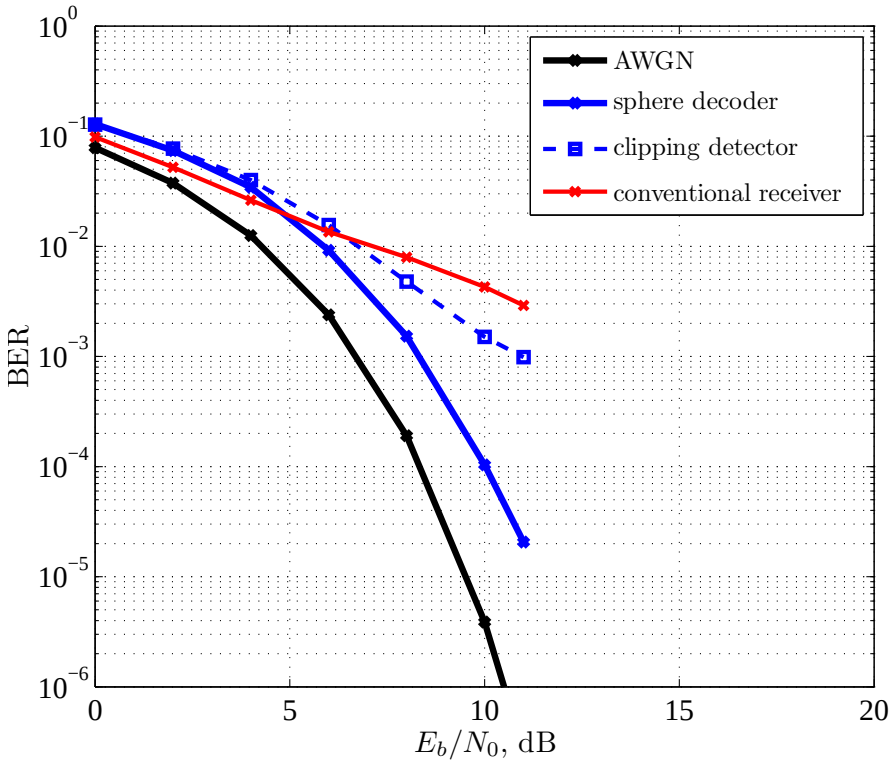


Figure 4.1: The BER Performance of the sphere decoder for an BPSK-OFDM system in DME interference for a single station with received peak power of 75 dBm and rate 10800 ppps

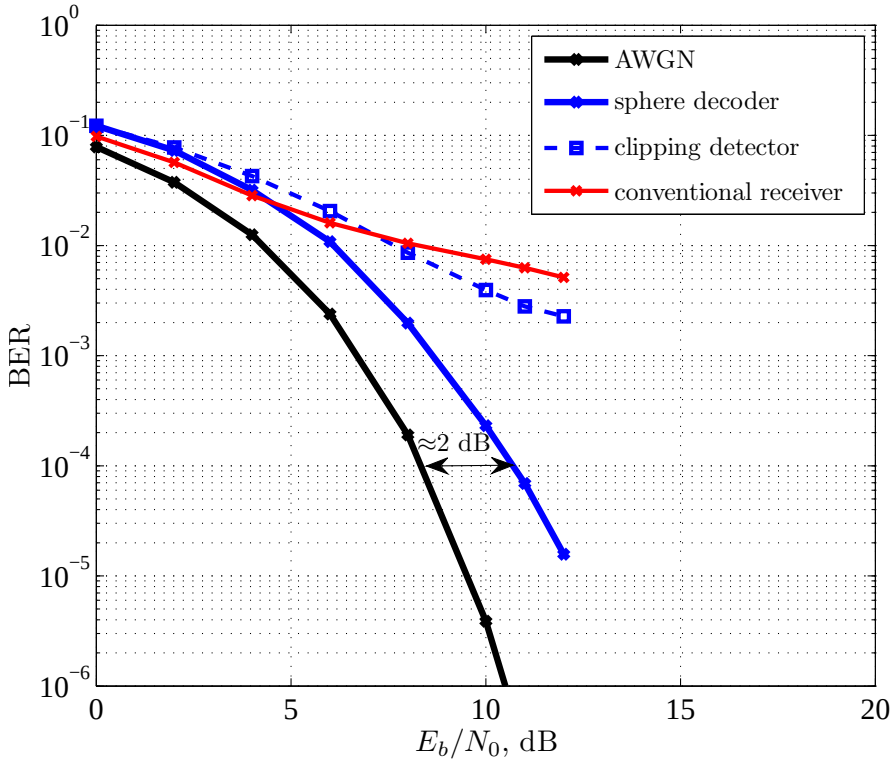


Figure 4.2: The BER Performance of the sphere decoder for an BPSK-OFDM system in DME interference for the worst case scenario

# Chapter 5

# Concluding Remarks

In this thesis, we have investigated the optimum detection schemes for L-DACS1 system in pulsed interference. In particular, we provided a statistical modeling of distance measuring equipment (DME) interference using a Gaussian mixture (GM) model. This modeling leads to suitable approximations of the optimum detection by determining noise states (Gaussian or impulsive) at the receiver. We then provided the optimum receiver design of orthogonal frequency division multiplexing (OFDM) systems in DME interference. From simulations, we found that the optimum OFDM receiver treats effectively the impacts of DME signals as impulse noise.

The first portion of this work concentrated on analyzing ans simulating the impacts of DME interference on the L-DACS1 system. Thus, we show that the outer subcarriers of the OFDM system are subject to strong impacts of the DME spectrum.
To cancel the effect of DME interference, we consider the statistical modeling of DME interference and AWGN. Herewith, we derived the relation between the DME pulses and the GM model. Therefore, we treat the effects of DME pulses and AWGN as GM interference. We showed that the GM model provides a good approximation to the voltage histogram of the received interference amplitude.
Lastly, we investigated the optimum receiver design for L-DACS1 system in GM interference. Under perfect knowledge of the location for the DME pulses, we showed that the optimum detector of OFDM signals reduces to a sphere decoder. The presented simulation showed that the proposed implementation for treating the impacts of DME interference provides a closed performance to a free-interference case.

# List of Acronyms

| | |
|---|---|
| AWGN | additive white Gaussian noise |
| BER | bit-error ratio |
| BPF | bandpass filter |
| BPSK | binary phase shift keying |
| CCDF | complementary cumulative distribution function |
| CP | cyclic prefix |
| DFT | discrete-Fourier transform |
| IDFT | inverse discrete-Fourier transform |
| MCA | Middleton Class-A |
| ML | maximum-likelihood |
| NSI | noise state information |
| OFDM | orthogonal frequency division multiplexing |
| PDF | probability density function |
| SNR | signal-to-noise ratio |

# Bibliography


[1] S. Brandes, I. Cosovic, and M. Schnell, "Reduction of out-of-band radiation in ofdm systems by insertion of cancellation carriers," *Communications Letters, IEEE*, vol. 10, no. 6, pp. 420–422, June 2006.

[2] K. Saaifan and W. Henkel, "Lattice signal sets to combat pulsed interference from aeronautical signals," in *Communications (ICC), 2011 IEEE International Conference on*, June 2011, pp. 1–5.

[3] M. Schnell, S. Brandes, S. Gligorevic, M. Walter, C. Rihacek, M. Sajatovic, and B. Haindl, "Interference mitigation for broadband l-dacs," in *Digital Avionics Systems Conference, 2008. DASC 2008. IEEE/AIAA 27th*, Oct 2008, pp. 2.B.2–1–2.B.2–12.

[4] K. A. Saaifan and W. Henkel, "Pulsed Interference Cancellation Based on Unused Spatial Dimensions and Lattice Signal Sets," 16$^{\text{th}}$ *International OFDM-Workshop*, August 2011.

[5] S. Brandes, U. Epple, S. Gligorevic, M. Schnell, B. Haindl, and M. Sajatovic, "Physical layer specification of the l-band digital aeronautical communications system (l-dacs1)," in *Integrated Communications, Navigation and Surveillance Conference, 2009. ICNS '09.*, May 2009, pp. 1–12.

[6] K. A. Saaifan, "Advanced Detection Schemes of Digital Signals in Impulse Noise," th *phD Thesis*, January 2015.

[7] D.-I. S. Brandes, "Suppression of Mutual Interference in OFDM Based Overlay Systems," 16$^{\text{th}}$ *phD Thesis*, May 2009.

[8] Z. Guo and P. Nilsson, "Algorithm and implementation of the K-Best sphere decoding for MIMO detection," *IEEE Journal on Selected Aera In Communications*, vol. 24, no. 3, pp. 491–503, 2006.

[9] K.-W. Wong, C.-Y. Tsui, R. S.-K. Cheng, and W.-H. Mow, "A VLSI architecture of a K-best lattice decoding algorithm for MIMO channels," in *IEEE International Symposium on Circuits and Systems*, May 2002.